https://dx.doi.org/10.1016/j.engstruct.2017.06.033

Mechanical Behaviour of Concrete-Filled CHS Connections Subjected to In-Plane Bending

Fei Xu[1,2], Ju Chen[1]* and Tak-Ming Chan[2]

1. Institute of Structural Engineering, Zhejiang University, Hangzhou, Zhejiang, 310058, P.R. China

2. Department of Civil and Environmental Engineering, The Hong Kong Polytechnic University, Hong Kong, 999077, P.R. China

Abstract: This paper presents an investigation on the mechanical behaviour of concrete-filled circular hollow section (CHS) connections. Four large-scale connection specimens were tested to failure under in-plane bending. The main test parameters included chord wall slenderness and diameter ratio between brace and chord. The main failure mode observed from the tests was chord-wall punching shear failure. Meanwhile the chord-wall deformation was also investigated to determine the governing limit state. Complementary finite element (FE) methodology was validated against the experimental findings and the validated FE models were used to further study the mechanical behaviour and the strength design of the connections. The modified Mohr-Coulomb criterion (MMC) was introduced into the finite element models to capture steel fracture failure. Based on both experimental and numerical investigations, a theoretical analytical model with the consideration of the inner concrete was established and an ultimate strength design equation was proposed accordingly to predict the punching shear strength for concrete-filled CHS connections under in-plane bending.

Keywords: Concrete-filled CHS connections; Experimental investigation; Numerical analysis; Design; Punching shear.

[1]Postdoctoral fellow, Department of Civil and Environmental Engineering, Hong Kong Polytechnic University, Hong Kong, P.R. China

[2]Associate Professor, Department of Civil Engineering, Zhejiang University, Hangzhou, P.R. China. (Corresponding author.) E-mail: cecj@zju.edu.cn

[3]Assistant Professor, Department of Civil and Environmental Engineering, The Hong Kong Polytechnic University, Hong Kong, P.R. China

1. Introduction

Concrete-filled steel tubular (CFST) structures are widely adopted in buildings, bridges, marine infrastructures and transmission towers. Inner concrete in a CFST member would significantly improve its local buckling resistance [1,2,3] especially for those with large diameter-to-thickness ratios. In transmission towers, poles and arch bridges [4], hollow or CFST chords and braces are commonly connected through welding. Previous research on the axial compressive [5-7] and tensile performance [6-9] of T-type concrete-filled CHS connections demonstrated that the capacity and radial stuffiness could be significantly improved when compared with the hollow section connections counterpart. These experimental investigation also showed that the typical failure modes of composite connections were brace failure [5,6] and crushing of inner concrete [5,7] in the case of axial compression and punching shear in the case of axial tension [6-9]. The inner concrete also prevents the inward tube-wall deformation thus enhancing the radial stiffness of the chord member, though not providing the direct tensile or compressive strength resistance to the external force. It can make full use of chord-wall material when the strength of brace is adequate as the connections fail at material level. The hollow horizontal branches welded to the CFST transmission poles will also support the gravity load of the electrical conductors and the ice-load, which will introduce in-plane bending to those connecting areas. However, limited studies [6] have been reported on the performance of in-plane bending loaded concrete-filled or grouted circular hollow section (CHS) connections.

In addition, current design code, AISC 360-10 [10], and guideline, CIDECT-1 [11], for tubular connections are primarily for hollow structural section (HSS) which mainly includes square hollow section (SHS) connections, rectangular hollow section (RHS) connections and CHS connections. By limiting the ratio of chord diameter to thickness (D/t) and selecting adequate material qualities and suitable welding procedures, the failure modes of plain steel HSS connections subjected to in-plane bending can be categorized into 1) chord punching shear (which is unlikely to occur without sufficient rotation capacity [12]) and 2) chord plasitification. The analytical model currently adopted in design codes and guidelines for punching shear failure assumes a full plastification of the punching shear area [12] with due account on the influence of chord-to-brace angle [11,13], whilst the design equations for

chord plastification in CIDECT-1 [11] are based on the modified function of Gerstein [14] and the analysis by van der Vegte *et al.* [15,16] and Qian *et al.* [17]. As for the concrete-filled connections, the design procedure given in CIDECT-3 [18] is based on the investigations of Packer and Fear [19] and Packer [7], applicable for concrete-filled SHS and RHS connections. Their investigations are based on Yield-line Theory. The design provisions for concrete-filled CHS connections subjected to in-plane bending is currently scarce. Therefore, this paper aims to develop design provisions for such connections through experimental, numerical and analytical studies. Based on the generated structural performance data and analytical studies, design equations are proposed.

2. Experimental Investigation

2.1. Test Specimens

Totally four specimens were tested under in-plane bending. The measured geometries (D, t, D_b, t_b) are shown in Table 1. The steel CHS tubes filled with self-compacting concrete were used for chord members, whilst the brace members were fabricated from plain CHS tubes. The nominal lengths of the chord and brace members were kept constant in all the test specimens and were 2000 mm and 630 mm, respectively. Fillet weld was used to connect the brace and chord in this test, as shown in Fig. 1.

The steel mechanical properties (yield strength – F_y, ultimate strength – F_u, elastic modulus – E_s and % of elongation at fracture – ε_f) were determined from tensile coupon tests, as summarized in Table 2. The 150-mm cubic compressive strength (f_{cu}) and elastic modulus (E_c) of inner concrete after 28 days were 56.3 MPa and 34,100 MPa, respectively. A 20-mm steel plate and stiffeners were welded on the top of brace member for MTS installation. Four connection specimens were tested in two days on the 28th and 29th after casting inner concrete.

The test specimens were labeled as the order of the connection type, the chord diameter, the chord-wall thickness, the brace diameter and the brace-wall thickness. For example, the label “T-300-4-133-6” defines a T-connection with a nominal outer chord diameter of 300 mm, nominal chord thickness of 4 mm, nominal outer brace diameter of 133 mm and nominal brace thickness of 6 mm.

2.2. Test Set-up and Loading System

Fig. 1 shows the details of test set-up and specimens under in-plane bending. The moment applied on test specimens was evaluated as the applied tension load multiplying its force arm 790 mm. Both ends of the chord were fixed and the brace end was connected to a 1,000kN-tension-capacity MTS actuator. The tensile load was controlled by the displacement of MTS load head at a constant speed of 0.5 mm/min for all test specimens. It could allow the tests to enter the post-failure stage. The chord wall deformations, 15 mm from the weld toe, were measured by LVDTs and the measurement arrangements are shown in Fig. 1. The date-acquisition frequency at 1 Hz was used during the whole test for the record of both applied load and displacements of transducers.

3. Test Results and Discussion

3.1. Failure Mode

The chord-wall punching shear failure at the crown of the tension side was the only failure mode observed in the tests. No obvious yield-line was observed on the chord wall near the weld toe until the load exceeded 85% of the ultimate strength. The initial fracture cracks formed at the chord-crown of the tension side and then developed quickly to the saddle sides along the weld toe. After a slight increase in the load (less than 3% of ultimate strength), these specimens finally failed in a sudden chord-wall fracture. The failure mode of composite connections was not affected by the chord wall slenderness (D/t) and diameter ratio between brace and chord (D_b/D) in these tests. The typical failure mode of specimens T-240-4-203-8 is shown in Fig. 2.

3.2. Chord-Wall Deformation

It is suggested in CIDECT-1 [11] for plain CHS connections under the strength limit state, the corresponding deformation at the peak loads in their load- deformation curves should be less than 3% D (0.03D), otherwise the connection capacity is the load corresponding to the deformation of 3% D (0.03D) which is called the deformation limit of 3% D. This is also applicable for a connection without a pronounced peak strength on its load-deformation curve. Additionally, the serviceability

deformation should be limited to 1% D (0.01D). The suitability of the recommendations was examined in this study.

The curves of load - deformation (Δ_B) which is the measured displacement difference between points B and B_1 (as shown in Fig. 1) for all the test specimens are plotted in Fig. 3 as solid lines. It is shown that the chord-wall thickness has some effects on its deformation. The deformation of specimens with 5-mm-chord-wall is less than those with 4-mm-chord-wall at the same load, while the maximum deformations were similar for connections with the same chord diameter.

In the test, the chord deformations at the peak load are less than the 3% deformation limit specified in the CIDECT-1 [11] recommendations for all specimens. The comparison is shown in Fig. 3. Although the maximum values exceed the serviceability deformation limit, 1% D (shown in Fig. 3), the service load is normally much less than the design strength. It is suggested by Lu e*t al.* [20] that the ultimate load was governed for the case of CHS connections because the ratios of limit strength to service strength (assuming the strength at deformation of 0.01D in this study) were always less than 1.5, which was also proved by the test results. If the load at the chord-wall deformation of 1% D is used for service strength according to CIDECT-1 in this investigation, the ratios of limit strength to service strength for this test series is 1.47 for specimens with D = 300 mm and 1.24 for specimens with D = 240 mm.

Therefore, the deformation limits recommended by CIDECT-1 [11] are generally satisfied.

3.3. Ultimate Strengths

The ultimate moment strengths ($M_{Exp} = F \times 630$ mm) of the test connections are shown in Table 1. It is slightly increased with the wall thickness for all test specimens.

AISC 360-10 design

In AISC 360-10 [10] specification, there are two limit states for plain steel CHS connections under in-plane bending, namely chord plastification and shear yielding (punching). The design strength equations are shown in Eqs. (1) and (2), respectively. The ultimate capacity, M_{AISC}, of a connection is determined by the lower one calculated from Eqs. (1) and (2).

Chord plastification (for T-connections under in-plane bending)

$$M_{\text{AISC, Plast}} = 5.39 F_y t^2 \gamma^{0.5} \beta D_b Q_f \quad (1)$$

Shear yielding (for T-connections under in-plane bending)

$$M_{\text{AISC, Punching}} = 0.6 F_y t D_b^2 \quad (2)$$

where F_y is the yield stress of the CHS member material, t is the wall thickness of the chord member, γ is the ratio of chord outer radius to chord thickness, β is the outer diameter ratio of brace to chord; D_b is the diameter of the brace member, Q_f is factors in the AISC 360-10 [10], $M_{AISC,Plast}$ and $M_{AISC,Punching}$ are the design strengths under the ultimate states of chord plastification and shear yielding, respectively.

The AISC 360-10 [10] design strengths (M_{AISC}) for plain steel CHS connections, the smaller ones calculated by Eqs. (1) and (2), are compared with the test results, as shown in Table 3. As anticipated, the comparison shows that if the participant of inner concrete is neglected, the connection design strengths are very conservative with an average M_{AISC}/M_{Exp} ratio of 0.32. According to the results calculated by AISC 360-10 [10], all the specimens are designed to fail at chord plastification, which is different from the test observations. Therefore, the AISC 360-10 [10] design strength at the ultimate state of shear yielding (punching) is also compared in Table 3. Similarly, these calculated punching shear strength by Eq. (2) are still conservative for all the specimens. This difference is due to the absence of the concrete contribution in evaluating the strengths. It should be noted that these two equations from AISC 360-10 [10] is intended to be valid for hollow structural section tubular connections only.

4. Finite Element Analysis

4.1. General Description

The finite element analysis (FEA) was conducted by ABAQUS/Explicit (6.10) [21] solution technique since it allows FE models to be discontinued which offers the possibility of visible “fracture crack” development when the material failure criterion is defined, by means of deleting elements from

mesh.

Solid element was used to model the steel tube since it enabled the feasibility in modeling the weld geometry which was irregular and could hardly be defined as a shell. In this study, the element type of C3D8R was chosen in both concrete and steel parts. The sensitivity analysis on mesh was conducted to find an appropriate element size with both accurate simulation result and acceptable computational time since element size would also affect the stable increment of FE model in ABAQUS/Explicit. The load-deformation curves of FE mode T-240-5-203-6 with the element sizes being 3 mm, 4 mm and 6 mm were compared. The number of elements was two along the thickness direction for the thickness of tube-wall less than 6 mm and for other cases it was three. For regions with more uniform stress profiles, the element size kept to be 25 mm. For the element size of concrete part, it was kept constant at 15 mm. The element size will mainly affect the fracture failure points of FE models, as shown in Fig. 4(a). The model with fine mesh tended to fail earlier than that with coarse one since the failure criterion was assumed to be activated upon one integration location of elements. Though fine mesh will not cause convergence problem in ABAQUS/Explicit, considering the computational efficiency and the aspect ratio of elements, the element size of 3 mm for the region near connecting area was adopted. Therefore the total number of elements was approximately 50,000 for the concrete part and 29,000 for the steel CHS connection part. Typical finite element mesh of concrete-filled CHS connection is shown in Fig. 5.

Though the convergence problem will not occur in ABAQUS/Explicit as mentioned before, we still should be aware of the stability of the simulation process when it is used in solving the quasi-static structural problem. So the ratio of all kinetic energy (ALLIK) and all internal energy (ALLIE) is used as an index to assess the suitability of relevant parameters and the rationality of simulation in this paper. To improve the computational efficiency without scarifying the calculation accuracy, a proper fixed mass scaling factor (MSF) was employed into the models at beginning which was preferred for quasi-static analysis [22]. The values of 10^4, 10^6, 10^9, 10^{10} and 10^{12} for fixed MSFs were evaluated by comparing their load-deformation curves, as shown in Fig. 4(b). In ABAQUS documentation, it is suggested that ratio of ALLIK to ALLIE should not exceed a small fraction value [22]. It was found

that large MSFs, i.e. 10^{12}, 10^{10}, 10^{9}, would cause unstable simulation process especially at the beginning stage. For models with fixed MSFs of 10^4 and 10^6, the ratios were both less than 5% and the load-deformation curves were almost coincided as shown in Figs. 4(b) and (c). However the computational time would be significantly reduced in the case of 10^6 by ten times theoretically when compared with the case of 10^4. Therefore the MSF value of 10^6 is adopted in the FEA.

For the steel constitutive model for chord and brace members, the plasticity properties were determined by true stress-strain curves obtained from the tensile coupon test results, with the von Mises yield criterion, associated flow rule and isotropic strain hardening. For the weld, an average size measured from test specimens was used. Since the failure would not occur at the weld which was design to be equal strength with members, its material property was the same as the chord. For the concrete constitutive model, constant values of 30°, 0.1, 1.16, 0.667 and 0.00025 were adopted in the concrete-damaged plasticity model (ABAQUS 6.10) for dilation angle (Φ_s), flow potential eccentricity (e_{con}), ratio of the compressive strength under biaxial loading to uniaxial compressive strength (f_{bo}/f_{co}), the ratio of the second stress invariant on the tensile meridian to that on the compressive meridian (K_c), and viscosity parameter (μ), respectively. The measured strength of concrete was used in defining the uniaxial stress-strain relationship by the concrete constitutive model suggested by Liang *et al*. [23]. The elastic modulus and Poison's ratio were taken as $4700\sqrt{f_c}$ [24] and 0.2 [25], respectively. The tensile behaviour of concrete was modeled by the fracture energy–based method suggested by CEB-FIP Model Code 2010 [26]. The interaction between steel and inner concrete was simulated by the contact interaction. The hard contact model and Coulomb friction model were employed in the normal and tangential directions, respectively. The value of the coefficient of friction μ was taken as 0.6 [27]. The boundary condition was set as the test where two chord-ends were fixed. The tensile load (parallel to the chord axis) was applied at the speed of 0.5 mm/min, as it in the test.

The modified Mohr-Coulomb (MMC) failure criterion with von Mises yield criterion [28], as shown in Eq. (3), was employed in finite element (FE) models to define the element failure using Metal Ductile Damage combined with user subroutine in ABAQUS/Explicit. The model assumes that

equivalent plastic strain at the onset of fracture damage ($\bar{\varepsilon}_{\mathrm{f}}$) is a function of stress triaxiality (η) and normalized Lode angle parameter ($\bar{\theta}$), as shown in Eq. (3). The criterion for fracture damage initiation is met when the condition that the damage index $\int_0^{\bar{\varepsilon}_{\mathrm{p}}} \frac{1}{\bar{\varepsilon}_{\mathrm{f}}(\eta,\bar{\theta})} d\bar{\varepsilon}_{\mathrm{p}}$ reaches 1.0 is satisfied [22], where the damage is assumed to accumulate with a linear incremental dependence on the equivalent plastic strain. The post-failure damage evolution was defined based on effective plastic displacement ($\bar{u}^{\mathrm{pl}}$) to mitigate the mesh-dependent for post-failure softening behaviour using * Damage Evolution [22]. Due to lack of experimental data, the effective plastic displacement at the point of element failure ($\bar{u}_{\mathrm{f}}^{\mathrm{pl}}$) set to be 0.1 in a linear evolution form according to ABAQUS Example problem guide [22]. In the FE model, an element would be removed from the mesh if $\bar{u}^{\mathrm{pl}}$ reaches $\bar{u}_{\mathrm{f}}^{\mathrm{pl}}$ at all of the section points at any one integration location of an element [22]. The MMC criterion can well predict the initial fracture crack and its propagation, especially for shear-dominated (low-triaxiality fracture) fracture [29]. It has been successfully applied to capture the punching shear failure for axial tensile loaded concrete-filled CHS connections [30].

$$\bar{\varepsilon}_{\mathrm{f}} = \left\{ \frac{A}{c_2} \left[\sqrt{\frac{1+c_1^2}{3}} \cos\left(\frac{\bar{\theta}\pi}{6} \right) + c_1 \left(\eta + \frac{1}{3} \sin\left(\frac{\bar{\theta}\pi}{6} \right) \right) \right] \right\}^{-\frac{1}{n}} \tag{3}$$

where $\bar{\theta}$ is the normalized Lode angle, η is the stress triaxiality, and $\bar{\varepsilon}_{\mathrm{f}}$ is the fracture equivalent strain.

There are four material parameters (A, n, c_1, c_2) need to be calibrated. The material strain-hardening parameters, A and n, can be calibrated from the true stress-strain curve fitting, using the Hollomon's power law equation, $\sigma = A\varepsilon^n$ [31]. The parameter of c_1 is a physical property parameter, "internal friction" coefficient, which is difficult to determine from conventional tensile coupon tests and will not vary too much for a material with similar crystallographic structures, so that it is determined according to the reference [29]. Three values of c_1 calibrated from material tests in reference [29] for 2024-T351 aluminum alloy, TRIP 690 and 780 steel with minimum ultimate stresses of 690 MPa and 780 MPa respectively, were adopted into the sensitive analysis shown in Fig. 6. The parameter of c_1 tend to affect the fracture initiation. Due to lack of material experimental data,

the c_1 value of TRIP 690 was employed in this study, where the yield stress and ultimate stress were most closed to the steel material used in this study compared with 2024-T351 aluminum alloy and TRIP 780 steel. Moreover, Fig.6 also shows that the connection strengths will change from -3.1% to 1.5% when the value changed from 0.1(-15%) to 0.14 (+15%), respectively. The parameter of c_2 is the maximum shear strength of steel materials determined from tensile coupon tests, expressed as 0.75 F_u [32]. Table 4 shows the values of four parameters for MMC criterion in numerical analysis.

4.2. Verification

To verify the developed finite element model, the ultimate loads obtained from the FEA results were compared with the test results in Table 5, with the corresponding mean value M_{FEA}/M_{Exp} of 0.97. It is shown that the FE model adequately predicted the ultimate strengths of the test specimens. Fig. 2 shows the comparison of typical failure mode between both FEA and test results. In addition, the curves of the load were plotted against the chord wall deformation obtained from the FEA and compared with the test results, as shown in Fig. 3. The numerical models captured well the general moment-deformation histories but may slightly overestimate and underestimate the fracture initiation for D = 240 mm and D = 300 mm specimens respectively. Nevertheless, these comparisons demonstrated that the developed finite element model is reliable.

Based on the validated finite element models, totally 220 FE models of connection subjected to in-plane bending with varying geometrical configurations and material properties were established in the parametric study. The chord length was kept constant at a value of 1400 mm and all other details such as the brace length, boundary conditions, interaction between steel and concrete and loading speed were kept the same with those verified test FE models, if not specially mentioned. In parametric study, to simulate the performance of connections with different steel grades, three stress-strain curves of different grade steel materials derived from tensile coupon tests were used in MMC criterion to obtain the parameters of n, A and c_2. The parameters of MMC criterion in the parametric study are presented in Table 4, whilst the material property of concrete was kept the same as the verified FE models.

5. Distribution of Punching Shear Stress

Fig. 7 shows the difference of the analytical model of sectional moment resistance between plain and concrete-filled CHS connections. For the plain CHS connection (Fig. 7(a)), it is assumed that the neutral axis locates on the center of the section, which is also the analytical model with uniform yield shear stress distributions on both compressive and tension sides for the punching shear design equation in AISC 360-10 [10]. While due to the participant of inner concrete in concrete-filled CHS connections, the neutral axis will move towards the compressive side. The analytical model for concrete-filled CHS connections is modified and presented in Fig. 7(b). The polar coordinates are introduced into this model for further shear strength profile description and connection strength calculation. In this section, the punching shear stress profile on the failure face are expressed as a piecewise function with an angle variable, θ. The locations of maximum shear stress in compressive side, neutral axis, and maximum shear stress in tension side are expressed in terms of three crucial parameters, θ_0, θ_1 and θ_2, respectively, as show in Fig. 7(b).

The shear stress distributions of moment loaded connections, T-240-4-110-6 and T-300-4-150-8, at the maximum load step were plotted in Fig. 8. Two parabolic functions are employed to describe the shear stress profile, as expressed in Eq. (4).

$$f_\tau = \begin{cases} \dfrac{\left|f_{\mathrm{v,cmax}}\right|}{\left(\theta_1-\theta_0\right)^2}\left(\theta-\theta_0\right)^2 - \left|f_{\mathrm{v,cmax}}\right| & 0 \le \theta < \theta_1 \\ -\dfrac{f_{\mathrm{v,tmax}}}{\left(\theta_2-\theta_1\right)^2}\left(\theta-\theta_2\right)^2 + f_{\mathrm{v,tmax}} & \theta_1 \le \theta \le \pi \end{cases} \tag{4}$$

where $f_{\mathrm{v,cmax}}$ and $f_{\mathrm{v,tmax}}$ are the maximum shear stresses at the compression and tension sides, respectively, θ is the angle parameter as shown in Fig. 7(b), θ_1 is the angle parameter of the position of neutral axis, and θ_0 and θ_2 are the angle parameters of the positions of $f_{\mathrm{v,cmax}}$ and $f_{\mathrm{v,tmax}}$, respectively.

6. Parametric study

The parametric study was conducted by the validated FE models to evaluate the values of angle parameters of θ_0, θ_1 and θ_2, which were constant for one specified connection. In order to better

understand these three vital angle parameters, the influence of geometric configurations on the shear stress values and profiles on the failure face were firstly assessed. Figs. 9(a), (b) and (c) show the shear stress distributions of connections with different values of geometric parameters, β (= D_b/D), γ (= $2D/t$) and τ (= t_b/t). It is shown that the parameters of β and γ have some effects on the maximum values of shear stress on both tensile and compressive sides and the position of neutral axial (θ_1) respectively, whilst the parameter τ has little effects on both shear stress values and profiles.

Furthermore, a total of 37 FE models of connections with the geometric parameters varied as follows: $0.20 \leq \beta \leq 0.60$, $30.0 \leq \gamma \leq 75.0$, $1.2 \leq \tau \leq 3.0$ were established and used to determine the angle parameters in Eq. (4). The results are shown in Fig. 10. It is shown that the values of θ_0, θ_1 and θ_2 ranged from 0.13π to 0.23π, 0.25π to 0.35π, and 0.63π to 0.73π, respectively. The approximate average values of each range, θ_0=0.18π, θ_1=0.3π, and θ_2=0.7π, are recommended in this study, meaning that the location of $f_{v,cmax,}$ neutral axis and $f_{v,tmax}$ can be defined by the angle parameters as shown in Fig. 7(b). The errors caused by this approximation can be less than ±10%. For example, the ultimate moment capacity of T-300-4-150-5 (f_u = 560MPa, in Table 6 and Line 13) calculated by equations using those mean values and curve-calibrated values of $0.178\ \pi$ (θ_0), 0.321π (θ_1) and 0.698π (θ_2) from numerical results are 43.34 kN·m and 41.19 kN·m respectively. It results in 5% difference.

7. Design Methods

7.1. Design philosophy

For the plain steel CHS connections, the in-plane bending design strength can be determined from the minimum strength value in the limit state from the two failure modes: 1) punching shear failure; and 2) chord plastification. However the chord plastification can be prevented in concrete-filled CHS connections, because the concrete in the chord effectively mitigates the inward deformation. Therefore, only the punching shear failure is considered.

7.2. Equivalent Thickness of Failure Face

An equivalent thickness method [30] is employed for design simplification. It is because the

thickness of the failure face varies at the whole chord-brace intersection curve. The spatial intersection curved surface of the failure face on the tension side is equivalent to cylindrical surface which is a plane circle with a thickness of T_{eq} perpendicular to the circle plane. The equivalent thickness of the tension side for connections under in-plane bending is thus modified, since only tension side is interested in the following proposed design equations, as shown in Fig. 11. The proposed equations are shown in Eqs. (5) and (6).

$$T_{eq} = \frac{S_t}{\Delta\theta\, D_b} = (1+\mu_{eq})t \tag{5}$$

$$\mu_{eq} = \frac{S_t}{\Delta\theta\, D_b\, t} - 1 \tag{6}$$

where T_{eq} is the equivalent thickness, S_t is the area of the failure face on the tension side, $\Delta\theta$ is the angle parameter (π-θ_1) indicating the tension side in Fig. 11, and μ_{eq} is defined as an equivalent area correcting parameter.

The coefficient μ_{eq} mainly varies with the parameter β (= D_b/D) which typically ranges between 0.2 and 0.8. The relationship between μ_{eq} and β is obtained from curve fitting with the calculated results, as shown in Fig. 12. The relationship thus can be expressed in an exponential function, as shown in Eq. (7).

$$\mu_{eq} = 0.7\beta^3 = 0.7(D_b / D)^3; \qquad 0.2 \le \beta \le 0.8 \tag{7}$$

7.3. Position of Resultant Force Point

(a) Compression side

Numerical results show that the von Mises stress distributions in the concrete reached the peak value near the chord crown and exhibited a good symmetry on the two sides of the peak value, as shown in Fig. 13. By integrating the first and second equations of Eq. (4) which represents the shear stress distribution on the compression and tension side respectively, the resultant shear force on both compression ($F_{c\text{-}steel}$) and tension sides (F_t) can be obtained. It is found that F_t is almost ten times of $F_{c\text{-}steel}$. As for the force equilibrium, resistant force provide by concrete ($F_{c\text{-}concrete}$) can be determined

as 0.9 F_t, where $F_{c\text{-}concrete}=F_t - F_{c\text{-}steel}=9\ F_{c\text{-}steel}=0.9\ F_t$, which means the inner concrete provides almost 90% of the resistant force on the compression side. Therefore, it is reasonable to assume that the resultant force point (O_c) of the compression side is located on the chord crown for simplification, as shown in Fig. 7(b). In addition, the value of the vertical distance from O_c to the neutral axis (Z_c) is $D_b(1-\cos\theta_1)/2 \approx 0.206D_b$.

(b) Tension side

The resultant force point on the tension side (O_t) is shown in Fig. 7(b). Substituting Eq. (4) and the value of Z_t can be calculated from Eq. (8).

$$Z_t = \frac{\iint_{\Sigma_{eq}} f_\tau z_t \mathrm{d}S_{eq}}{\iint_{\Sigma_{eq}} f_\tau \mathrm{d}S_{eq}} \approx 0.533D_b \tag{8}$$

where Z_t is the vertical distance from O_t to the neutral axis, S_{eq} is the equivalent calculation area determined above, as shown in Fig. 11, and z_t is the vertical distance from the calculation point to the neutral axis.

(c) Internal lever arm of the section

The internal lever arm of the moment section is the sum of Z_c and Z_t. The value of Z_t calculated from Eq. (8) is approximately equal to $0.533D_b$. Therefore the internal lever arm can be determined to be $0.739D_b$ ($=Z_c+ Z_t$), which is equivalent to 0.658π expressed by angle parameter (θ_t), shown in Fig. 7(b). To simplify the calculations, θ_t can be taken as $2/3\pi$, and then the internal lever arm can be determined as follows:

$$Z = \frac{D_b}{2}(1-\cos\theta_t) = \frac{3}{4}D_b \tag{9}$$

7.4. Maximum Shear Stress

From the experimental observations, the punching shear failure (shear-dominated fracture) has been shown to govern the mechanical behaviour of the connections. In most cases, the load corresponding to the first through thickness fracture crack was the maximum strength of the

connections. The first failed element reaches the maximum shear stress ($f_{v,tmax}$) under the triaxial stress state corresponding to the equivalent plastic strain on the fracture criterion failure surface. In fact, the $f_{v,tmax}$ is lower than the ultimate shear strength ($f_{u,v}$) determined under the pure shear stress state. It is because the existence of normal stress caused by chord bending will adversely affect the failure shear stress of one element. The $f_{v,tmax}$/ $f_{u,v}$ ratio for the first failed element is plotted against the connection strengths obtained from the FEA results in Fig. 14. Generally, $f_{v,tmax}$ is 88% $f_{u,v}$ (0.88 $f_{u,v}$) among 21 finite element models.

7.5. Design Equation

The ultimate strength at the shear-dominated fracture failure for the plain or concrete-filled CHS connections under in-plane bending is considered as the sum of the shear stress multiplying its vertical distance to the neutral axis on the failure face. The specified analytical model is shown in Fig. 7(b). Eq. (10) is proposed to calculate the ultimate strength:

$$M_u = \iint_{\Sigma_{eq}} f_\tau z_\theta \mathrm{d}S_{eq} = F_{V,t} \times Z \tag{10}$$

where M_u is the ultimate moment strength, f_τ is shear stress distribution function, expressed by Eq. (4), $F_{V,t}$ is the total shear force of the failure face on the tension side, expressed by Eq. (11), and Z is the internal lever arm, expressed by Eq. (9).

The value of $F_{V,t}$ can be calculated by integral Eq. (4) on the failure face in tension side. Substituting Eq. (4), the $F_{V,t}$ can ultimately be written as Eq. (11).

$$\begin{aligned} F_{V,t} &= \iint_{\Sigma_{eq}} f_\tau \mathrm{d}S_{eq} = (1+\mu_{eq}) D_b\, t \int_{\theta_1}^{\pi} f_\tau(\theta)\mathrm{d}\theta \\ &= \frac{49}{96}\pi(1+\mu_{eq})\, f_{v,tmax}\, D_b\, t \end{aligned} \tag{11}$$

As shown earlier, $f_{v,tmax}$ can be taken as 88% of the ultimate shear strength $f_{u,v}$, that is $f_{v,tmax}$= 0.88 $f_{u,v}$ = 0.88 ×0.75F_u [32]. Then, by substituting Eqs. (7), (9) and (11), Eq. (10) can be rewritten as Eq. (12).

$$M_u = \left(0.79 + 0.56\left(\frac{D_b}{D}\right)^3\right) F_u\, D_b{}^2\, t \tag{12}$$

where M_u is the ultimate moment strength; D_b is the brace diameter; D is the chord diameter; F_u is the steel ultimate tensile strength for the chord; t is the chord wall thickness.

The ultimate strengths predicted by Eq. (12) for T-connections (M_u) are compared with the experimental and FEA results in Tables 5 and 6, with the mean value of M_u/M_{Exp} (Table 5) and M_u/M_{FEA} (Table 6) being 0.68 and 0.80, respectively. In general, Eq. (12) gives a conservative prediction for the ultimate in-plane bending strength of the composite T-connections. This result may be attributed to neglecting the effects of the weld in the proposed equation. If the weld width, as shown in Figs. 2 and 7, is considered by including the width into the calculation for an equivalent fracture failure area and an internal lever arm, the mean values of M_{u_Weld}/M_{Exp} and M_{u_Weld}/M_{FEA} are 0.82 (Table 5) and 0.98 (Table 6), respectively. In addition, FE models without welds were also established and the results were compared with the corresponding calculated strengths from the proposed equation. The comparison between numerical and calculated results, as shown in Table 6, demonstrates a good correlation with the mean value of M_u/M_{FEA} being 0.97. Despite this, the weld cannot be neglected during the investigation of shear stress distribution and mechanical behaviour, since the presence of weld will affect the geometry of failure face and shear stress profile.

However the influence of weld width will significantly decrease as the brace diameter increases, the absence of weld width in capacity calculation can be considered as the safety reserve for the sudden tube-wall fracture failure. Besides that, the accurate weld width is difficult to consider. Therefore, it is reasonable to recommend Eq. (12) as a design equation. It should be noted that some parameters used the deduction procedure for the proposed design equation, Eq. (12), are derived from numerical analysis. Therefore the applicable range should be in accordance with the parametric study, namely $0.20 \leq \beta \leq 0.60$, $30.0 \leq \gamma \leq 75.0$.

8. Conclusions

Experimental and numerical studies were conducted on the mechanical behaviour of concrete-filled CHS connections subjected to in-plane bending. All the test specimens were failed in punching shear failure mode, since the inner concrete could effectively restrain the inward chord wall deformation.

Therefore deformation limits recommended by CIDECT-1 [11] could be satisfied. It has been shown that the inner concrete effectively supports the chord wall in compression side, which means the contribution from the concrete should be considered in the sectional moment resistance. On the basis of both experimental and numerical investigations, new design equations based on metal fracture mechanism for concrete-filled CHS connections under in-plane bending were proposed. The actual shear stress distributions, the effects of curved failure faces and the participant of inner concrete in the sectional resistance were considered in the proposed design equation. The comparison indicated that the design predictions agreed well with both the test and FEA results.

Acknowledgments

The research work described in this paper was supported by the research project from the Science and Technology Department of Zhejiang Province (2015C33005). The first and third authors are also grateful for the support from the Chinese National Engineering Research Centre for Steel Construction (Hong Kong Branch).

References

[1] O'Shea MD, Bridge RQ. Design of thin-walled concrete filled steel tubes. J Struct Eng 2000; 10.1061/(ASCE)0733-9445(2000)126:11(1295), 1295-1303.

[2] Uy B. Local and postlocal buckling of fabricated steel and composite cross sections. J Struct Eng 2001; 10.1061/(ASCE)0733-9445(2001)127:6(666), 666–677.

[3] Bradford MA, Loh HY, Uy B. Slenderness limits for filled circular steel tubes. J Constr Steel Res 2002; 58(2), 243-252.

[4] Chen BC, Wang TL. Overview of concrete filled steel tube arch bridges in China. Practice periodical on structural design and construction-ASCE 2009; 14(2), 70-80.

[5] Feng R, Young B. Tests of concrete-filled stainless steel tubular T-joints. J Constr Steel Res 2008; 64(11): 1283-1293.

[6] Tebbett IE, Beckett CD, Billington CJ. The punching shear strength of tubular joints reinforced with a grouted pile. Offshore Technology Conference 1979; 915–921.

[7] Packer JA. Concrete-filled HSS connections. J Struct Eng 1995; 121(3): 458-467.

[8] Xu F, Chen J, Jin WL. Experimental investigation and design of concrete-filled steel tubular CHS connections. J Struct Eng 2015, 10.1061/(ASCE)ST.1943-541X.0001050, 04014106.

[9] Huang W, Fenu L, Chen B, et al. Experimental study on K-joints of concrete-filled steel tubular truss structures. J Constr Steel Res 2015; 107, 182-193.

[10] ANSI/AISC 360-10. Specification for structural steel buildings. Chicago, USA: America Institute of Steel Construction (AISC); 2010.

[11] Wardenier J, Kurobane Y, Packer JA, van der Vegte GJ, Zhao X-L. Design guide for circular hollow section (CHS) joints under predominantly static loading, 2nd Ed., CIDECT-1. Comité International pour le Développement et l'Étude de la Construction Tubulaire, LSS Verlag, Germany; 2008.

[12] Wardenier J. Hollow section joints. Delft University Press, Delft, Netherlands; 1982.

[13] API RP2A-WSD. Recommended practice for planning, designing and constructing fixed offshore platforms, 23nd. Washington D.C., USA: American Petroleum Institute (API), 23nd, 2014.

[14] Gibstein MB. The static strength of T-joints subjected to in plane bending. Det Norske Veritas report 76-137; 1976.

[15] van der Vegte GJ, Wardenier J, Qian XD, Choo YS. Reanalysis of the moment capacity of CHS joints. Proceedings 12th International Symposium on Tubular Structures, Shanghai, China, Tubular Structures XII, Taylor & Francis Group, 579-588; 2008.

[16] van der Vegte GJ, Wardenier J, Zhao X-L, Packer JA. Evaluation of new CHS strength formulae to design strengths. Proceedings 12th International Symposium on Tubular Structures,

Shanghai, China, Tubular Structures XII, Taylor & Francis Group, 313- 322; 2008.

[17] Qian XD, Choo YS, van der Vegte GJ, Wardenier J. Evaluation of the new IIW CHS strength formulae for thick-walled joints. Proceedings 12th international symposium on tubular structures, Shanghai, China, Tubular sturectures XII, Taylor & Francis Group, 271-280; 2008.

[18] Packer JA, Wardenier J, Zhao X-L, van de Vegte GJ, Kurobane Y. Design guide for rectangular hollow section (RHS) joints under predominantly static loading, 2nd Ed., CIDECT-3. Comité International pour le Développement et l'Étude de la Construction Tubulaire, Verlag TÜV Rheinland. Cologne, Germany; 2009.

[19] Packer JA, Fear CE. Concrete-filled rectangular hollow section X and T connections. Proc. 4th Int. Symp. on Tubular Structures, Delft University Press, Netherlands, 382–391; 1991.

[20] Lu LH, de Winkel GD, Yu Y, Wardenier J. Deformation limit for the ultimate strength of hollow section joints. Proc. Sixth International Symposium on Tubular Structures, Melbourne, Australia; 341-7; 1994.

[21] *ABAQUS 6.10* [Computer software]. Dassault systemes, Waltham, MA, USA; 2010.

[22] Hibbitt H D, Karlsson B I, Sorensen P. ABAQUS documentation collection. Ver.6.10, USA; 2010.

[23] Liang QQ, Fragomeni S. Nonlinear analysis of circular concrete-filled steel tubular short columns under axial loading. J Constr Steel Res 2009; 65(12): 2186-2196.

[24] ACI (American Concrete Institute) Committee 318. Building Code Requirements for Structural Concrete (ACI 318-11) and Commentary (ACI 318R-11). Farmington Hills, MI, USA: ACI; 2011.

[25] Hu HT, Huang CS, Wu MH, Wu YM. Nonlinear analysis of axially loaded concrete-filled tube columns with confinement effect. J Struct Eng 2003; 129(10): 1322-1329.

[26] FIB. CEB-FIP Model Code 2010-Final draft, Vol.1. Lausanne, Switzerland: federation internationale du béton; 2012.

[27] Han LH, Yao GH, and Tao Z. Performance of concrete-filled thin-walled steel tubes under pure torsion. Thin Wall Struct 2007; 45(1), 24-36.

[28] Bai Y, Wierzbicki T. Application of extended Mohr-Coulomb criterion to ductile fracture. Int J Fract 2010; 161(1): 1-20.

[29] Bai Y, Wierzbicki T. A comparative study of three groups of ductile fracture loci in the 3D space. Eng Fract Mech 2015; 135: 147-167.

[30] Xu F, Chen J, Jin WL. Punching shear failure of concrete-filled steel tubular CHS connections. J Constr Steel Res 2016, 124:113-121.

[31] Hollomon JH. Tensile deformation. Trans AIME 1945; 12: 268-290.

[32] John MA, Franklin DJ, Henry HR. Guide to the use of tables and formulas in machinery's handbook, 28th Ed., Industrial Press, New York, USA; 2008.

Notation

The following symbols are used in this paper:

A = parameters of material strain hardening;

c_1 = friction coefficient in Mohr-Coulomb model;

c_2 = shear stress resistance in Mohr-Coulomb model;

D = outer diameter of the chord member;

D_b = outer diameter of the brace member;

e_{con} = flow potential eccentricity in the concrete damaged plasticity model;

E_s = Young's modulus of steel;

E_c = Young's modulus of concrete;

f_{bo}, f_{co} = initial equibiaxial compressive yield stress and initial uniaxial compressive yield stress in the concrete damaged plasticity model;

f_c = concrete compressive design strength;

f_{cu} = concrete compressive cube strength;

$f_{u,v}$ = ultimate shear strength of steel;

$f_{v,cmax}$ = the maximum shear stress on the punching shear face at the compression side;

$f_{v,tmax}$ = the maximum shear stress on the punching shear face at the tension side;

f_τ = shear stress distribution on the punching shear face;

F_y = yield strength of steel;

F_u = ultimate strength of steel;

$F_{V,t}$ = the total shear force on the tension side of the failure face;

K_c = ratio of the second stress invariant on the tensile meridian to that on the compressive meridian in the concrete damaged plasticity model;

M_{AISC} = ultimate bending strength calculated from AISC 360-10;

M_u = design ultimate bending strength calculated using the proposed equation;

M_{Exp} = ultimate moment load obtained from experimental results under in-plane bending;

M_{FEA} = ultimate bending strength obtained from FEA;

M_{u_Weld} = design ultimate bending strength calculated using the proposed equation considering the weld width;

n = parameters of material strain hardening;

Q_f = coefficient specified in the AISC 360-10;

S_t = the total area of the punching shear failure face at the tension side;

Z = internal lever arm of the moment section;

t = chord-wall thickness;

522 t_b = brace-wall thickness;

523 Teq = equivalent thickness;

524 $\bar{u}^{pl}$ = effective plastic displacement;

525 $\bar{u}_p^{pl}$ = effective plastic displacement at the failure point;

526 ε_f = elongation (tensile strain) after fracture based on a gauge length of 50 mm;

527 $\bar{\varepsilon}_f$ = the equivalent strain at the point of fracture;

528 $\bar{\varepsilon}_p$ = the equivalent strain;

529 Δ_B = measured chord wall deformation at point B in Fig. 1.

530 β = ratio of brace outer diameter to chord outer diameter;

531 γ = ratio of chord outer radius to chord thickness;

532 τ = ratio of brace thickness to chord thickness;

533 θ = the angle parameter defined in Fig. 7(b);

534 $\bar{\theta}$ = Lode angle parameter (normalized Lode angle);

535 θ_0, θ_1, θ_2 = the position of fv,cmax, neutral axis and fv,tmax expressed by the angle parameter in Fig.
536 7(b), respectively;

537 μ = viscosity parameter in the concrete damaged plasticity model;

538 μ_{eq} = a coefficient related to S_t, D_b and t;

539 Φ_s = dilation angle measured in the p-q plane in the concrete damaged plasticity model;

540 η = stress triaxiality.

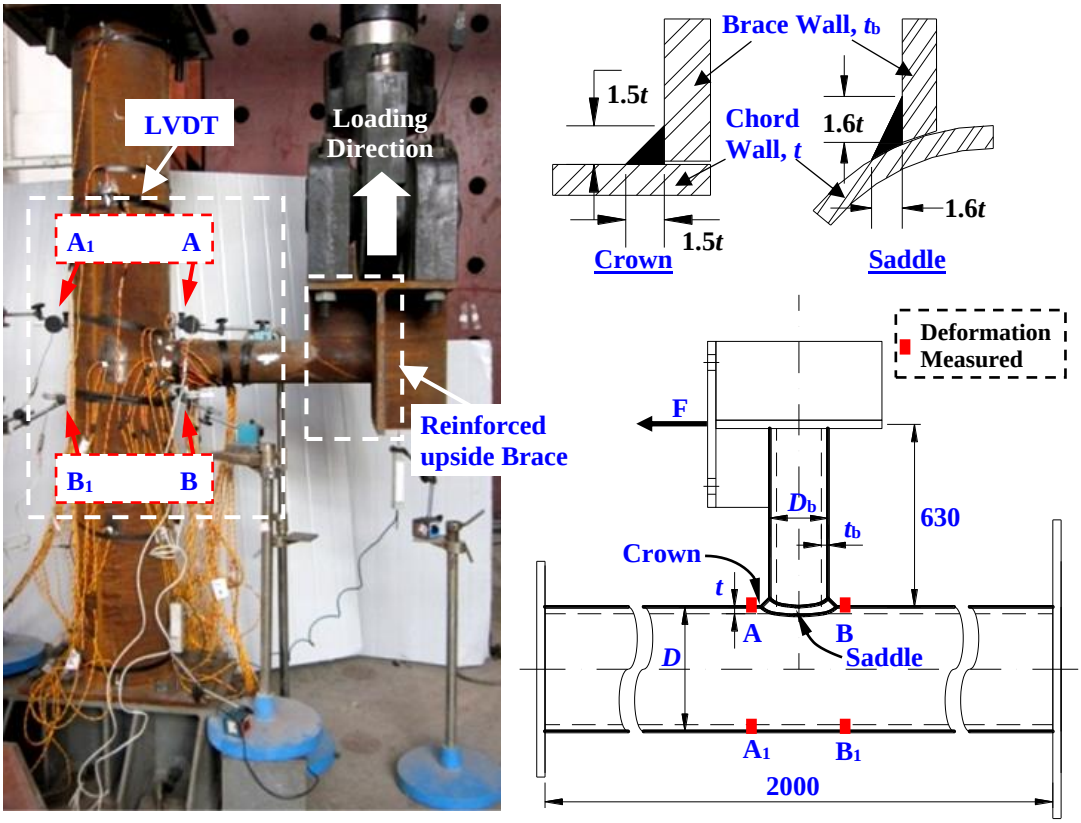

Fig. 1 Test set-up for specimens subjected to in-plane bending (Unit: mm)

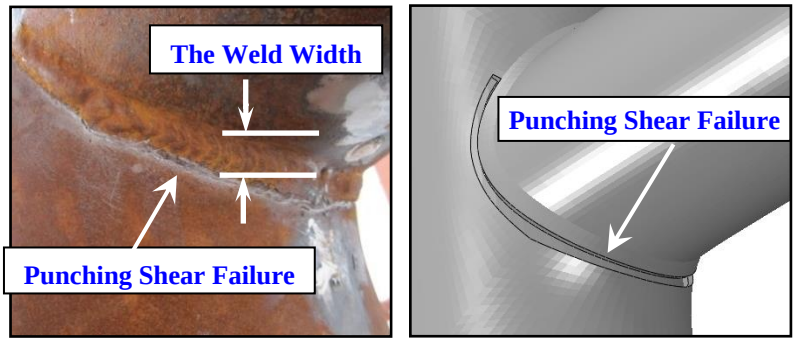

Fig. 2 Failure mode of test specimen T-240-4-203-8

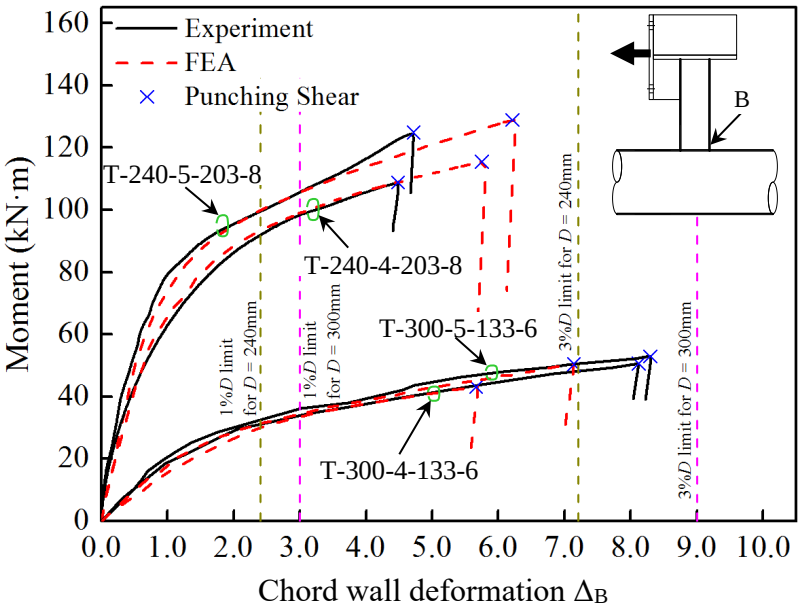

Fig. 3 Moment-deformation curves for test specimens

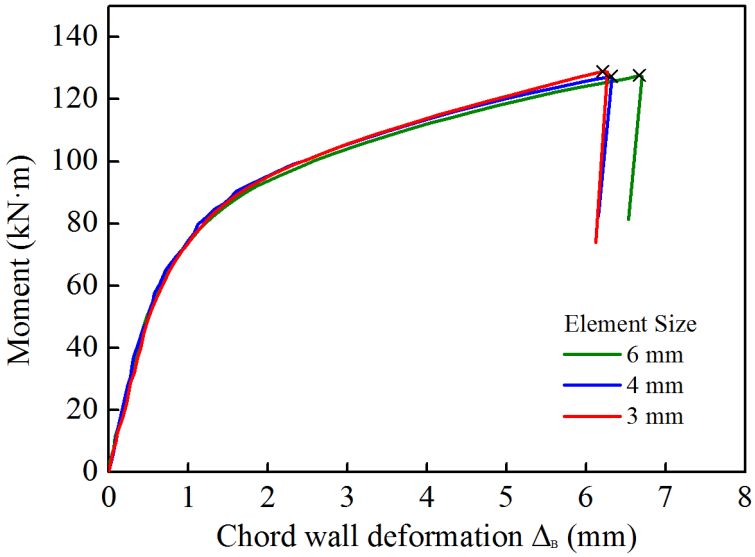

(a) Mesh sensitive analyses

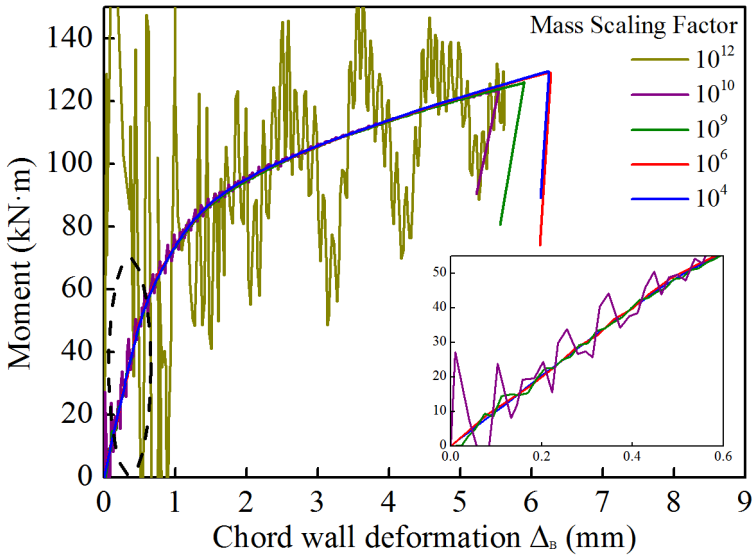

(b) MSF sensitive analyses

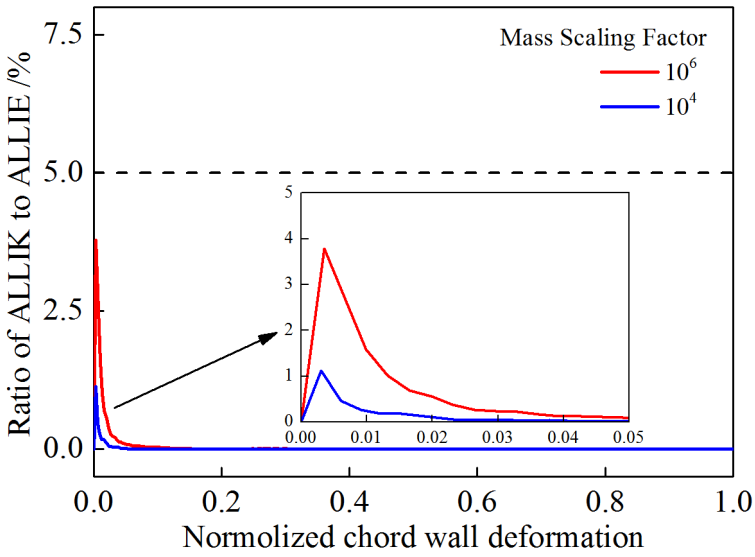

(c) Ratio of ALLIK to ALLIE

Fig. 4 Sensitive study of model parameters (T-240-5-203-6)

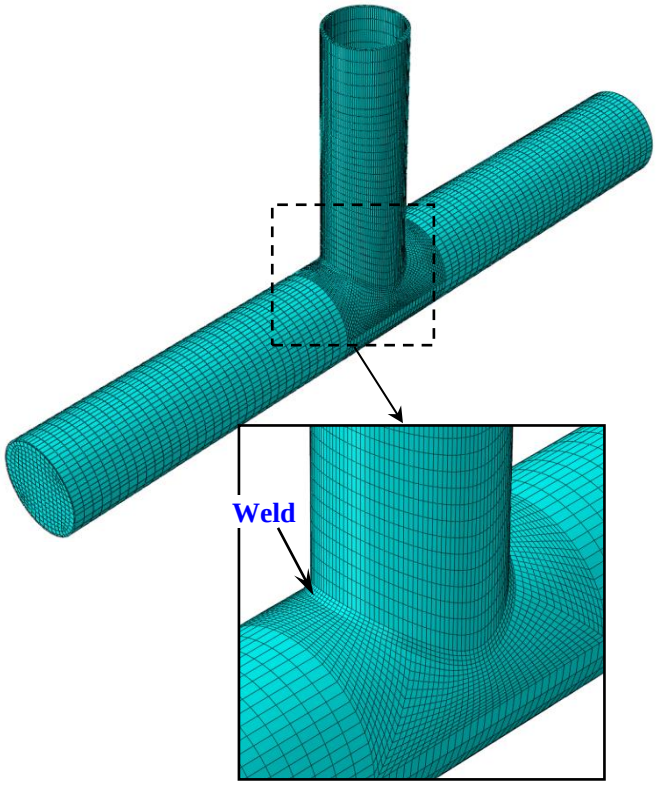

Fig. 5 Finite element model

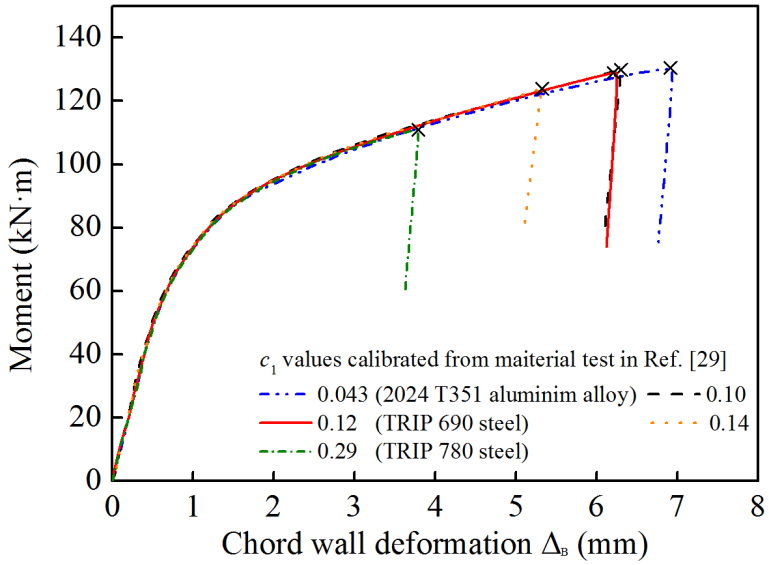

Fig. 6 Effect of c_1 on the results of numerical models

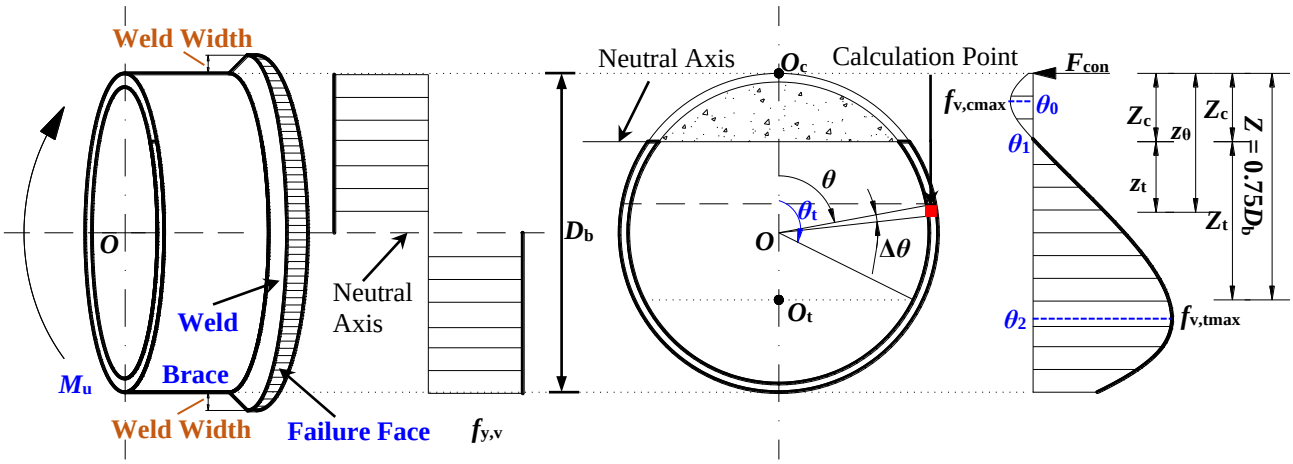

(a) Plain CHS connection (b) Concrete-filled CHS connection

Fig. 7 Analytical model of punching shear for in-plane bending connections

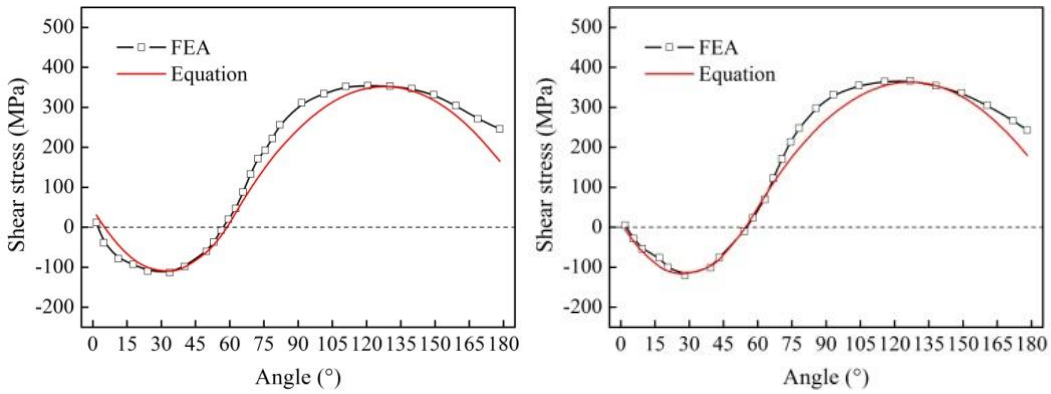

(a) T-240-4-110-6 (b) T-300-4-150-8

Fig. 8 Shear stress distribution in the punching shear failure face

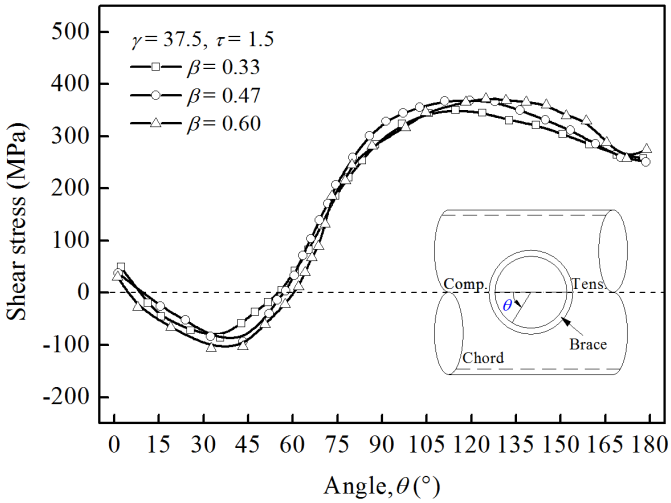

(a) Diameter ratio of brace to chord, β

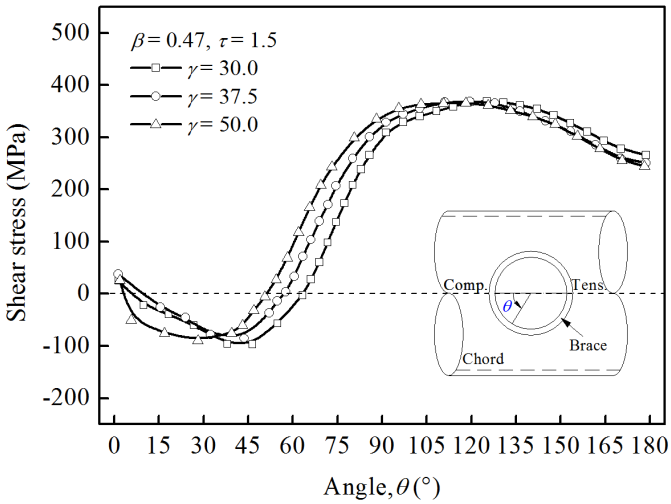

(b) Ratio of chord diameter to radius, γ

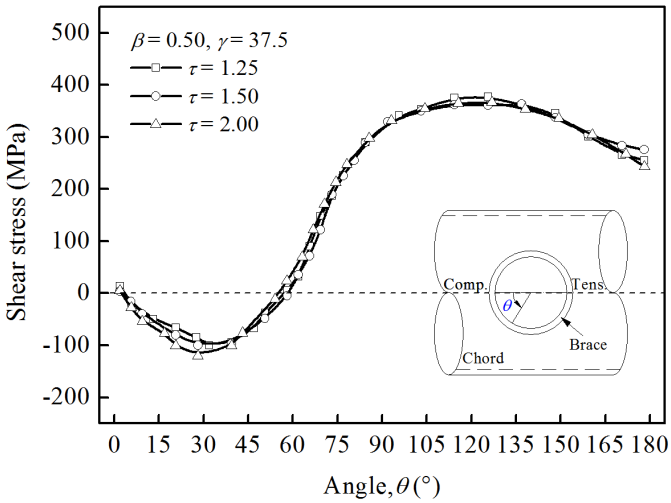

(c) Tube-wall thickness ratio of brace to chord, τ

Fig. 9 Influence of geometric configurations on the shear stress distribution

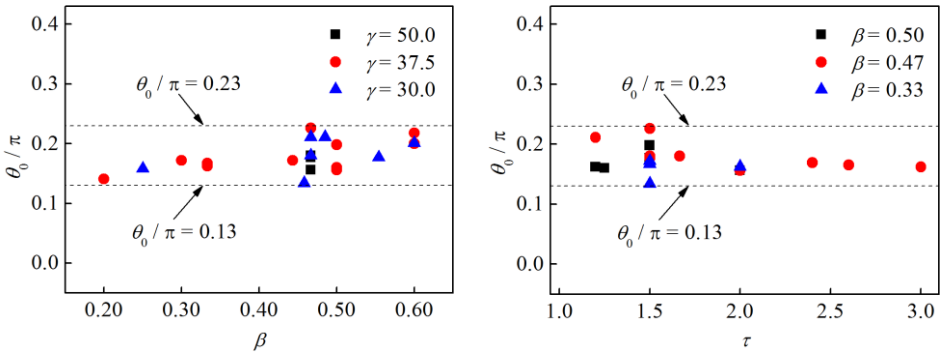

(a) Values of parameter θ_0 for T-connection FEA model

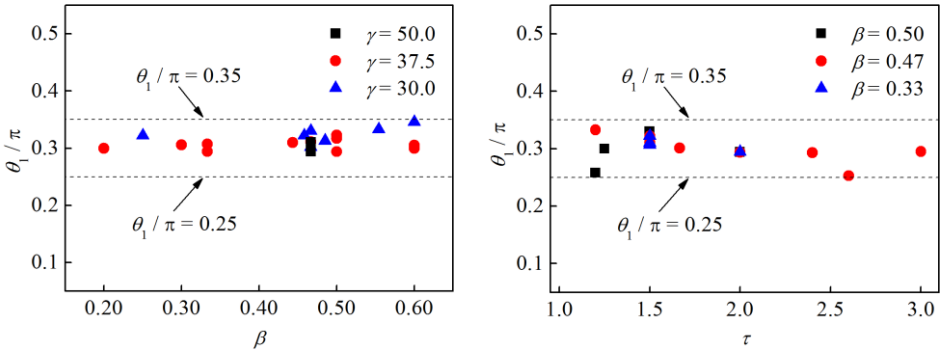

(b) Values of parameter θ_1 for T-connection FEA model

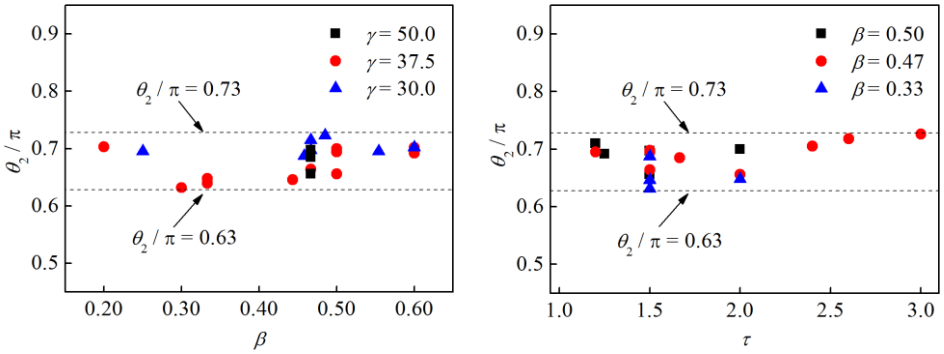

(c) Values of parameter θ_2 for T-connection FEA model

Fig. 10 Parametric study on angle parameters

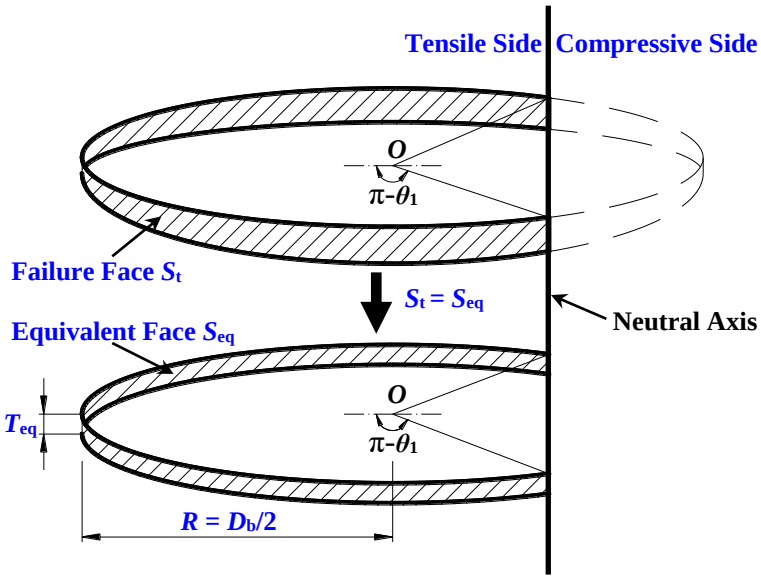

Fig. 11 Equivalent punching shear failure face

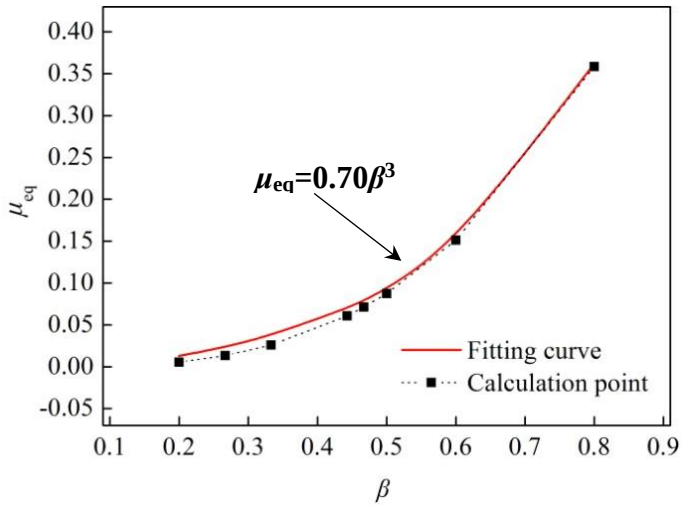

Fig. 12 Effect of β on equivalent area correcting parameter μ_{eq}

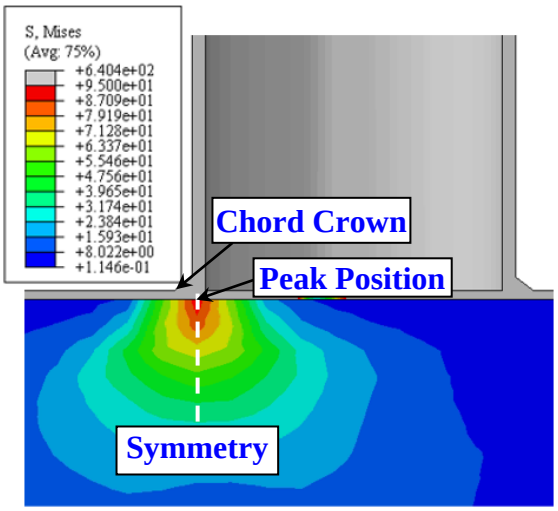

(a) T-300-5-140-6

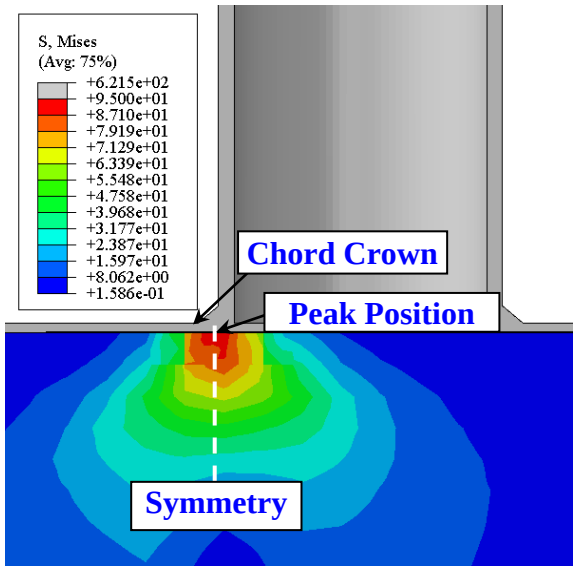

(b) T-240-4-110-6

Fig. 13 The von Mises stress distribution in the inner concrete on the compression side

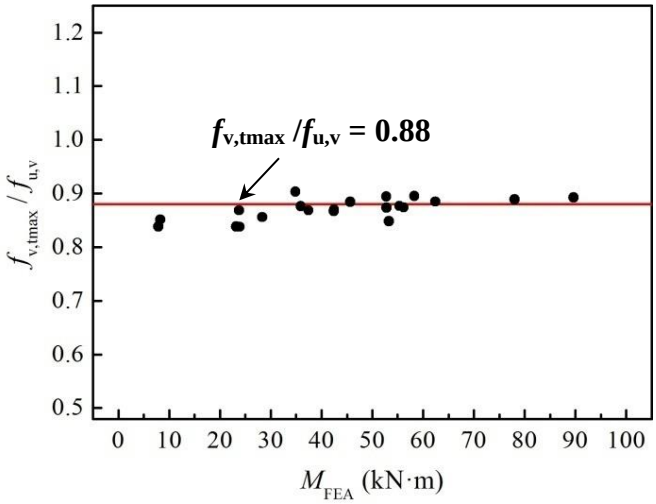

Fig. 14 Ratios of $f_{v,tmax}$ to $f_{u,v}$

Table 1. Measured geometries, ultimate strengths and failure modes of the test specimens

Specimens	Chord		Brace			L_b	β	M_{Exp}	Failure
	D	t	L	D_b	t_b			kN·m	mode
	mm	mm	mm	mm	mm	mm			
T-300-4-133-6	298.8	4.09	2002.1	134.2	6.08	630.2	0.449	50.72	CPS
T-300-5-133-6	301.3	5.04	2001.8	133.9	6.09	630.4	0.444	52.98	CPS
T-240-4-203-8	238.8	3.93	2001.3	201.9	8.07	630.1	0.845	108.90	CPS
T-240-5-203-8	241.2	4.95	2000.9	204.1	8.06	630.1	0.846	124.93	CPS

Note: D: Outer diameter of the chord, t: Wall thickness of the chord, L: length of the chord, D_b: Outer diameter of the brace, t_b: Wall thickness of the brace L_b: length of the brace, β: the chord diameter ratio D_b/D, and CPS: Chord punching shear.

Table 2. Measured mechanical properties of the test specimens

Steel	Nominal thickness (mm)	F_y (MPa)	F_u (MPa)	E_s (GPa)	ε_f (%)
Q345 (Chord)	4.0	452	547	2.04×10^5	27.7
Q345 (Chord)	5.0	385	513	2.04×10^5	31.8
Q345 (Brace)	6.0	408	549	2.00×10^5	32.0
Q345 (Brace)	8.0	436	520	2.02×10^5	33.7

Table 3. Comparison of the AISC 360-10 strengths and the test results for connections subjected to in-plane bending

Specimens	M_{Exp} (kN·m)	M_{AISC} (kN·m)	$M_{AISC,Punching}$ (kN·m)	$\frac{M_{AISC}}{M_{Exp}}$	$\frac{M_{AISC,Punching}}{M_{Exp}}$
T-300-4-133-6	50.72	14.07	19.19	0.28	0.38
T-300-5-133-6	52.98	16.75	20.43	0.32	0.39
T-240-4-203-8	108.90	36.66	44.70	0.34	0.41
T-240-5-203-8	124.93	43.64	47.60	0.35	0.38
			Mean	0.32	0.39

Table 4. Parameters of MMC criterion used in finite element models

Steel			F_y (MPa)	F_u (MPa)	Coefficients			
					c_1	c_2 (MPa)	A (MPa)	n
In validated FE models	Chord	4.0 mm	452	547	0.12	410.3	865.5	0.163
		5.0 mm	385	513	0.12	384.8	845.0	0.181
	Brace	6.0 mm	408	549	0.12	411.8	882.3	0.179
		8.0 mm	436	520	0.12	390.0	822.5	0.161
In parametric study models			298	427	0.12	320.3	693.7	0.207
			450	560	0.12	420.0	836.2	0.141
			495	640	0.12	480.0	951.2	0.139

Table 5. Comparison of the proposed design strengths to both FEA and test results

Specimens	M_{Exp} kN·m	M_{FEA} kN·m	M_u kN·m	M_{u_Weld} kN·m	M_{FEA} / M_{Exp}	M_u / M_{Exp}	M_{u_Weld} / M_{Exp}
T-300-4-133-6	50.72	43.11	32.46	38.81	0.85	0.64	0.77
T-300-5-133-6	52.98	50.36	38.06	45.50	0.95	0.72	0.86
T-240-4-203-8	108.90	115.32	101.79	120.03	1.06	0.93*	1.10*
T-240-5-203-8	124.93	128.96	119.32	140.71	1.03	0.96*	1.13*
				Mean	0.90	0.68	0.82

*Note: The value of β for these specimens are beyond the application scope of proposed equations, therefore they are not used in calculating the mean value.

Table 6. Comparison of proposed design strengths and FEA results

Specimens	F_y (MPa)	F_u (MPa)	M_{FEA} (kN·m)	M_u (kN·m)	M_{u_Weld} (kN·m)	M_u /M_{FEA}	M_{u_Weld} /M_{FEA}
T-300-4-60-6	450	560	8.28	6.41	8.70	0.77	1.05
T-300-4-100-6	450	560	23.18	18.16	22.74	0.78	0.98
T-300-4-100-8	450	560	23.89	18.16	22.74	0.76	0.95
T-300-4-133-6	450	560	42.48	33.24	40.81	0.78	0.96
T-300-2-140-6	450	560	23.76	18.59	22.66	0.78	0.95
T-300-3-140-4.5	450	560	34.88	27.89	34.00	0.80	0.97
T-300-3-140-6	450	560	35.90	27.89	34.00	0.78	0.95
T-300-4-140-6	298	427	37.45	28.35	34.56	0.76	0.92
T-300-4-140-6	450	560	45.67	37.18	45.33	0.81	0.99
T-300-4-140-6	495	640	52.76	42.49	51.80	0.81	0.98
T-300-5-140-6	450	560	56.19	46.48	56.66	0.83	1.01
T-300-5-140-7.5	450	560	58.31	46.48	56.66	0.80	0.97
T-300-4-150-5	450	560	52.79	43.34	52.37	0.82	0.99
T-300-4-150-6	450	560	53.27	43.34	52.37	0.81	0.98
T-300-4-150-8	450	560	55.32	43.34	52.37	0.78	0.95
T-300-4-180-6	298	427	62.42	50.41	59.78	0.81	0.96
T-300-4-180-6	450	560	78.04	66.11	78.40	0.85	1.00
T-300-4-180-6	495	640	89.63	75.56	89.60	0.84	1.00
T-240-4-60-6	450	560	8.92	6.44	8.78	0.72	0.98
T-240-5-60-6	450	560	9.98	8.05	10.98	0.81	1.10
T-240-3-110-6	450	560	23.43	17.16	21.38	0.73	0.91
T-240-4-110-6	450	560	28.36	22.87	28.51	0.81	1.01
T-240-3-133-6	450	560	33.71	26.31	32.94	0.78	0.98
T-240-4-133-6	450	560	42.4	35.08	43.92	0.83	1.04
T-240-5-133-6	450	560	50.34	43.85	54.9	0.87	1.09
T-300-4-60-6*	450	560	6.65	6.41	N/A	0.96	N/A
T-300-4-100-6*	450	560	19.15	18.16	N/A	0.95	N/A
T-300-4-140-6*	450	560	37.73	37.18	N/A	0.99	N/A
T-300-4-150-8*	450	560	44.68	43.34	N/A	0.97	N/A
					Mean	0.80	0.99
					COV	0.043	0.046
					Mean*	0.97	N/A
					COV*	0.016	N/A

* Note: FE models of connections without welds.